



## Simultaneous quantum and classical communication via multiparameter modulation

Piao Tan <sup>1</sup>, Tao Wang <sup>2,\*</sup>, Huanxi Zhao,<sup>2</sup> Zicong Tan,<sup>2</sup> Peng Huang,<sup>2</sup> and Guihua Zeng<sup>2,3,†</sup>

<sup>1</sup>Northwest University, Xi'an 710127, Shaanxi, China

<sup>2</sup>State Key Laboratory of Advanced Optical Communication Systems and Networks, Center of Quantum Sensing and Information Processing, Shanghai Jiao Tong University, Shanghai 200240, China

<sup>3</sup>College of Information Science and Technology, Northwest University, Xi'an 710127, Shaanxi, China



(Received 20 November 2023; accepted 4 March 2024; published 25 March 2024)

Classical and quantum communication protocols share similarities in terms of signal modulation, transmission, and reception, providing a basis for their integration. The integration of these protocols can lead to high-efficiency and low-cost performance by utilizing a single set of communication infrastructures to simultaneously achieve continuous-variable quantum key distribution and classical communication on a single wavelength. In this paper, we propose a simultaneous quantum and classical communication (SQCC) protocol based on multiparameter modulation, which combines pulse position modulation (PPM) for classical communication and Gaussian-distributed modulation (GM) for quantum key distribution, named GMCS-PPM-SQCC protocol. Classical information is transmitted using the arrival time parameter of the coherent state, while quantum key information is distributed through the two quadrature components of the coherent state. Coherent detection is used to detect all three parameters, and different data processing schemes are utilized to extract the corresponding information. We verified the feasibility of the protocol through simulations, discussed its secure transmission distance, bit error rate, and secret key rate in realistic scenarios. Our protocol has better phase noise tolerance than traditional SQCC protocol. It can further facilitate the integration of classical and quantum communication, and contributes to the deployment and application of QKD.

DOI: [10.1103/PhysRevA.109.032621](https://doi.org/10.1103/PhysRevA.109.032621)

### I. INTRODUCTION

Continuous-variable quantum key distribution (CV-QKD) is one quantum key distribution (QKD) protocol that utilizes the quadrature components of the optical field to transmit quantum key information securely between the sender Alice and the receiver Bob. The security of CV-QKD is based on the fundamental principles of quantum physics [1–3]. One of the most widely studied protocols for CV-QKD is the Gaussian modulated coherent-state (GMCS) protocol, which is theoretically and practically secure [4–13]. GMCS-CV-QKD has advantages in co-fiber transmission and antibackground light noise due to its encoding and detection characteristics. Recent advances in CV-QKD have led to improvements in transmission distance [14,15], secret key rate (SKR) [16,17], chip realization [18–20], and networking deployment [21], which have facilitated the engineering application of this technology.

The integration of QKD with classical communication can effectively reduce the overall implementation cost of QKD. Wavelength-division multiplexing (WDM) is a widely adopted method to achieve this integration. By utilizing WDM and filters, high-speed classical optical signals and quantum signals in discrete-variable QKD (DV-QKD) can be transmitted simultaneously, as demonstrated in various studies (see, e.g., Refs. [22–24]). Similarly, the WDM technique has also been employed in CV-QKD for achieving integration.

However, although WDM enables the merging of physical channels for transmission, the devices at both ends of the transceiver still remain as two independent sets of devices, thereby limiting the extent of integration.

Enhancements at the protocol level can overcome the aforementioned limitations and enable the integration of classical and quantum communication. To this end, Qi *et al.* proposed the simultaneous quantum and classical communication (SQCC) protocol, which utilizes a single coherent state to superimpose quantum information onto classical information [25]. One of the key advantages of this protocol is that only one set of transceivers is needed to transmit both types of information, thereby obviating the need for a dedicated channel for QKD. This feature makes the SQCC protocol particularly appealing for achieving CV-QKD in a coherent optical communication system at a minimal cost [26]. However, this protocol is subject to limitations arising from phase noise, which ultimately determines the maximum transmission distance under the true local oscillator (LO) design. To address this issue, Qi *et al.* proposed the use of simultaneously generated reference pulses to compensate for phase drift and demonstrated experimentally that this approach could meet the phase alignment requirement of the SQCC protocol [27]. Nonetheless, the requirement for phase correction remains high. In addition, it is necessary to accurately calibrate the channel transmittance, to ensure an accurate separation of classical and quantum information, which could pose a practical security issue.

In optical communication, the light wave possesses multiple parameters, such as amplitude, phase, polarization

\*tonystar@sjtu.edu.cn

†ghzeng@sjtu.edu.cn

direction, and arrival time, which can be utilized to transmit bit information. For instance, pulse position modulation (PPM) employs the arrival time of an optical pulse to convey classical information. Specifically, in PPM, each frame consists of multiple time slots, and the position of the optical pulse within a slot encodes classical information. Building on this concept, we can employ one optical pulse to transmit classical bits, while the remaining slots are utilized for quantum key information transmission. This multiparameter modulation approach enhances the spectrum utilization efficiency of PPM and further reduces the implementation complexity of QKD. In addition, different parameters are used to transmit information, which can be better separated at the receiver, and can completely avoid the separation difficulty of classical information and quantum information on the same parameter.

In this paper, we present an SQCC protocol based on multiparameter modulation, named GMCS-PPM-SQCC protocol, which combines PPM for classical communication and Gaussian-distributed modulation for CV-QKD. In particular, classical information is transmitted using the arrival time parameter of the optical pulse, while CV-QKD employs the two quadrature component parameters of the coherent state for distributing quantum key information. We evaluate the practical feasibility of this protocol through simulations and analyze its secure transmission distance, bit error rate (BER), and SKR. With a repetition frequency set at 250 MHz and a signal power level of 1500 SNUs, this protocol can transmit classical information over a distance of 50 km with a BER below  $1 \times 10^{-9}$ . Additionally, the SKR for quantum key information can be transmitted at a rate of 1.34 Mbps over the same 50 km distance. In comparison, with a signal power of 1500 SNUs, the SKR performance of the traditional SQCC protocol is significantly lower than that of the GMCS-PPM-SQCC protocol, reaching only 0.67 Mbps at a distance of 15 km, due to the impact of phase noise.

This paper is structured as follows: In Sec. II, we review the conventional CV-QKD protocol and the conventional SQCC protocol and introduce the GMCS-PPM-SQCC protocol with emphasis on its unique characteristics. Furthermore, a qualitative analysis of the strengths and limitations of this protocol is presented. In Sec. III, we present the results of a numerical simulation of the GMCS-PPM-SQCC protocol based on actual system parameters. Finally, we presented a discussion in Sec. IV and conducted a conclusion in Sec. V.

## II. PROTOCOL DESCRIPTION

### A. GMCS-CV-QKD protocol

Among various CV-QKD protocols, the GMCS protocol has gained the most popularity due to its proven security. The GMCS protocol has been successfully demonstrated in real-world CV-QKD networks, and the security distance can exceed 200 km using this protocol [28,29]. GMCS-CV-QKD leverages the classical coherent optical communication framework for QKD. The protocol can employ time division multiplexing, frequency division multiplexing, and polarization multiplexing techniques to separate LO and quantum signals effectively. The specific process for using the GMCS-CV-QKD protocol is as follows:

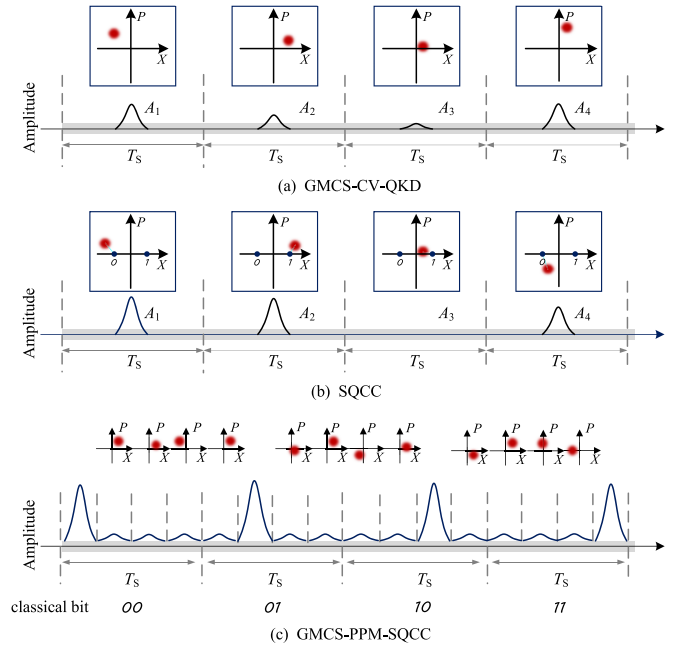


FIG. 1. Phase-space representations and amplitude of various modulation formats. (a) GMCS-CV-QKD modulation format. (b) Traditional SQCC modulation format. (c) GMCS-PPM-SQCC modulation format.

(1) Alice first randomly generates two Gaussian random sequences  $\{X_A\}$  and  $\{P_A\}$ , with the mean of 0, variance of  $V_A$ , and the length of  $n$ . Then, she prepares  $n$  coherent states  $\{|X_A + iP_A\rangle\}$ . The prepared coherent states are sent to Bob through the quantum channel. With the channel transmittance as  $T$  and the excess noise as  $\varepsilon$ , the channel noise measured from the input of Bob is  $1 + \varepsilon T$  and the total noise of channel line is  $\chi_{\text{line}} = (1 + \varepsilon T)/T - 1 = 1/T + \varepsilon - 1$  [3], which is introduced in the transmission process of the coherent state.

(2) After Bob receives the coherent state, two quadrature components are measured simultaneously by heterodyne detection, and obtain  $\{X_B\}$  and  $\{P_B\}$ . The quantum efficiency in the heterodyne detector is  $\eta$ , and the electronic noise of the detector is  $V_{\text{el}}$ . Heterodyne detection requires two detectors, so the total noise of detection is  $\chi_{\text{het}} = [1 + (1 - \eta) + 2V_{\text{el}}]/T$ . Alice and Bob then keep all the modulation data and received data, respectively.

(3) Alice randomly selects part of the data and makes the data public. Bob precalibrates the quantum efficiency  $\eta$ , the electronic noise  $V_{\text{el}}$ , modulation variance  $V_A$ , the total channel noise  $\chi_{\text{line}}$  and the total detection noise  $\chi_{\text{het}}$  can be obtained, and then evaluates the crucial parameters such as channel transmittance  $\hat{T}$  and the excess noise  $\hat{\varepsilon}$  according to the measurement data. Finally, the secure transmission distance and SKR can be evaluated through the calculation in the Appendix.

(4) Finally, Alice and Bob conduct data postprocessing on the remaining data through classic authentication channels, and finally obtain the security key for subsequent data encryption.

Figure 1(a) illustrates the phase-space representations and time-domain pulse sequences in GMCS-CV-QKD. The

coherent-state signal in the phase space exhibits a Gaussian probability distribution for both quadrature components, and its amplitude is proportional to the power of the pulsed light, which is also directly proportional to the mean photon number. Each coherent-state pulse occupies a time interval of  $T_s$ .

### B. Traditional SQCC protocol

In this section, we introduce the traditional SQCC protocol, which concurrently encodes classical information and quantum information onto quadrature component, employing a single coherent state for the transmission of both classical and quantum information [25].

Specifically, Alice first selects the modulation formats for classical communication and CV-QKD. Assuming binary phase shift keying (BPSK) modulation is utilized for classical communication and Gaussian modulation is utilized for CV-QKD, the specific process of this protocol is

(1) Alice proceeds to assign the quadrants of the coherent states in the phase space based on her classical bits, followed by determining the specific positions of the coherent states based on the corresponding Gaussian random numbers. For example, Alice generates classical bit  $m_A$  ( $m_A \in 0, 1$ ) and Gaussian distribution random numbers  $\{X_A, P_A\}$ , and uses them to prepare  $n$  coherent states  $|(X_A + e^{-im_A\pi}\alpha) + i(P_A + e^{im_A\pi}\alpha)\rangle$ , where  $\alpha$  is the amplitude of classical communication.

(2) Upon receiving the coherent state, Bob first identifies the classical bit based on the quadrants, then removes the displacement resulting from the classical modulation, and subsequently retrieves the superimposed Gaussian data [as depicted in Fig. 1(b)]. Specifically, at Bob, the two quadrature components  $X_R$  and  $P_R$  are measured simultaneously by heterodyne detection. When Bob detects  $X_R(P_R) > 0$ , the classical information  $m_B = 0$ . Otherwise, the value of  $m_B$  is assigned the value one. The measurement result of quantum key information is

$$\begin{aligned} X_B &= \frac{X_R}{\sqrt{\eta T}} + (2m_B - 1)\alpha, \\ P_B &= \frac{P_R}{\sqrt{\eta T}} + (2m_B - 1)\alpha. \end{aligned} \quad (1)$$

(3) Through  $\{X_A, X_B\}$  and  $\{P_A, P_B\}$ , Alice and Bob can undertake further postprocessing to generate a secure key [25].

This scheme enables classical bits and random keys of QKD to be encoded on the same weak coherent states, and detected by the same coherent receiver, so that each coherent state can simultaneously carry the key and classical information. However, the implementation of this scheme faces two primary challenges:

(1) First, it demands high precision in phase correction, requiring the phase deviation to be at the level of  $10^{-3}$ . However, on the one hand, the randomly generated QKD signal is regarded as a noise in the classical signal. To reduce the BER of the classical signal transmission, the amplitude of the classical modulation needs to be increased. On the other hand, because the classical signal is superimposed with the QKD signal, the higher the amplitude of the classical signal modulation, the greater the excess noise will be generated due

to the phase jitter of the coherent states, thus affecting the transmission performance of CV-QKD [27].

(2) Separation of classical information and quantum information is crucial since both are modulated on the quadrature components of the physical quantity. While power calibration can be achieved through parameter estimation with large datasets, this aspect requires further investigation. Currently, the classical signal power at the receiver end is set to a constant to facilitate information decomposition. However, this may lead to inaccuracies in information separation in scenarios involving changes in channel transmittance or the QKD device's own losses.

Therefore, when the protocol is implemented, the overall protocol performance will be degraded due to the performance of the actual device.

### C. GMCS-PPM-SQCC protocol

Herein, we extended the traditional SQCC protocol and proposed the GMCS-PPM-SQCC protocol, which uses arrival time parameters and quadrature component parameters to carry different information. Specifically, classical data is encoded via the time parameter of the highest optical pulse, while quantum key information is encoded via the quadrature components of the coherent state. Encoding through the arrival time of optical pulses corresponds to the PPM modulation format in classical optical communication, which is a prevalent modulation technique employed in deep-space optical communications. Quadrature component modulation corresponds to IQ modulation in classical optical communication. The corresponding modulation format and pulse position are shown in Fig. 1(c).

The specific process of using GMCS-PPM-SQCC protocol is as follows:

(1) In Alice, we employ PPM on the prepared coherent states and classical optical pulses. Specifically, in PPM, the interval between symbols is  $T_s$ , which can be equally decomposed into  $L$  time slot. Here  $L$  represents the number of positions where pulses appear, which satisfies  $L = 2^n$  with the encoding bit number  $n$ . Therefore, PPM can be represented as L-PPM based on the number of encoded bits. In Fig. 1(c),  $L$  takes 4, and its encoding bit determines the time interval position of its highest optical pulse occurrence. In 4-PPM modulation, when the highest optical pulse occupies the first to fourth time slot, the classic bit information is 00, 01, 10, 11, respectively.

(2) Then, Alice performs Gaussian modulation on the remaining three time slots, and prepares coherent states  $\{|X_A + iP_A\rangle\}$  within these three time slots. The preparation of these coherent states aligns with the GMCS protocol. Within the prepared signal, each frame comprises one classical optical pulse and three coherent states, which are transmitted to Bob.

(3) After receiving the signal at Bob, PPM demodulation and heterodyne detection is performed on the signal. Classical information is judged according to the arrival time of the high pulse within a time interval  $T_s$ . In one symbol interval, when the power of one time slot is greater than the power of the other slots in the time domain, the classic bit information can be determined. Then, the determined classical bit information

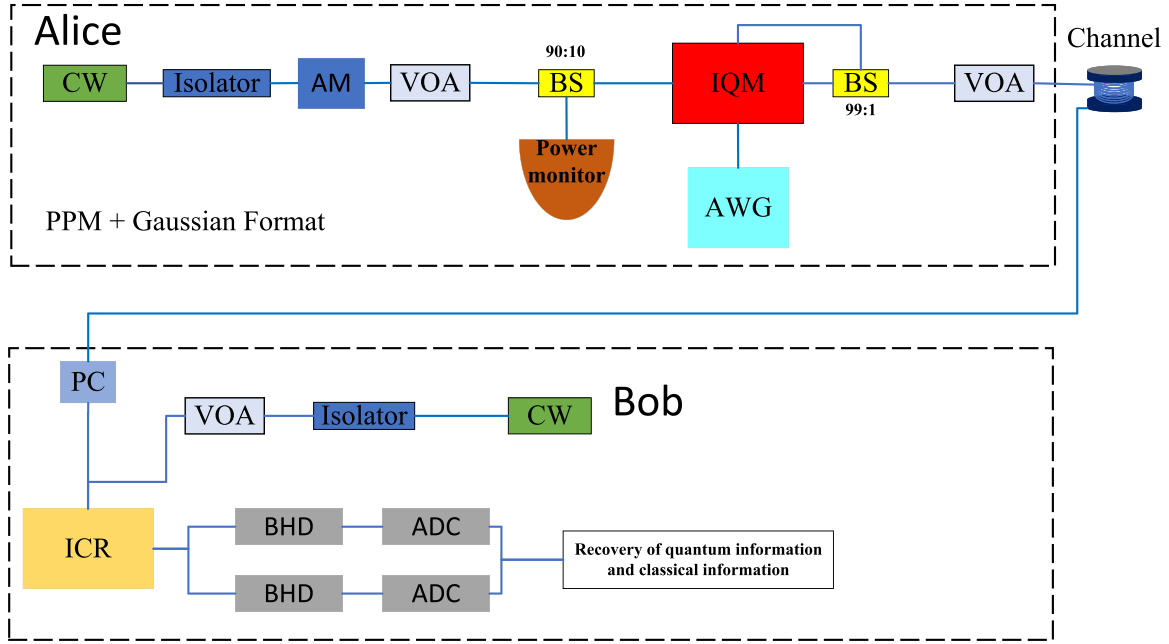


FIG. 2. GMCS-PPM-SQCC protocol flow chart. CW: continuous-wave laser; AM: amplitude modulator; VOA: variable optical attenuator; BS: beam splitter; IQM: IQ modulator; AWG: Arbitrary waveform generators; PC: polarization controller; ICR: integrated coherent detector; BHD: balanced homodyne detector; ADC: Analog-to-digital converter.

is removed and the remaining Gaussian data  $\{X_B, P_B\}$  is extracted.

(4) Alice and Bob can further calculate the SKR from the original data  $\{X_A, P_A\}$  and  $\{X_B, P_B\}$ , which is consistent with the traditional GMCS-CV-QKD, and ultimately extract the secure key.

This protocol can be implemented as depicted in Fig. 2. In particular, at Alice, a continuous-wave (CW) laser is successively connected to an isolator and an amplitude modulator (AM), ensuring forward transforming of optical signals through the isolator and changing to optical pulse signals via the AM. To control optical power, the optical pulses pass through a variable optical attenuator (VOA). Subsequently, the optical pulses are divided into two beams using a 90 : 10 beam splitter (BS), with one beam serving for power monitoring and the other being directed into an IQ modulator (IQM). The arbitrary waveform generators (AWG) then performs PPM and IQ modulation on the optical pulse. Notably, the IQM is connected to a 99 : 1 BS, which is utilized to extract a portion of the optical pulse for controlling the bias voltage of the IQM. Finally, the signal is attenuated to achieve the desired optical power level using a VOA and transmitted to Bob through an optical fiber channel. At Bob, the received optical signal undergoes polarization control using a polarization controller (PC). Simultaneously, a CW laser emits a LO light under the protection of an isolator, which is attenuated to the appropriate power level through a VOA. Subsequently, the optical signal and the LO light are mixed within an integrated coherent detector (ICR) and realize heterodyne detection, ultimately facilitating the recovery of both classical information and quantum information.

The GMCS-PPM-SQCC protocol offers the following advantages: First, using different parameters to encode makes information easy to distinguish, which makes classical

information and quantum information easy to be extracted. Second, classical information is no longer affected by phase noise, although the quadrature component of the quantum signal is still affected by phase deviation. The third point is that in longer distance transmission, especially in deep-space communication, the performance of PPM modulation is better than orthogonal amplitude-phase modulation, so its classical communication performance will be better.

However, due to bandwidth allocation for classical communication in GMCS-PPM-SQCC protocol, the symbol rate of CV-QKD is slightly lower than that of traditional SQCC. All in all, the initial concept behind our proposed protocol is to encode information by utilizing various parameters of the coherent state. One can also consider implementing this protocol by combining the polarization state with quadrature components. In the following section, we use simulations to estimate the performance of the proposed scheme.

### III. PERFORMANCE ANALYSIS

In GMCS-PPM-SQCC protocol, the noise generated during the concurrent transmission of quantum and classical communication can impact the protocol's performance. To assess and evaluate the protocol's effectiveness, in this section, specialized noise analyses are separately conducted for classical communication and CV-QKD. Subsequently, calculate the BER for classical communication and the SKR for CV-QKD, utilizing simulated results generated with common typical parameters.

#### A. Noise analysis

During the transmission of GMCS-PPM-SQCC protocol, quantum Gaussian state and classical signal are merged within



each frame. Our protocol employs the time slots containing high-pulse signals for the transmission of classical information, while utilizing coherent states in the remaining slots for the transmission of quantum key information. Throughout the entire transmission process, with regard to the transmission of classical signals, quantum signals are considered as Gaussian additive noise due to their occupation of other time slots, leading to misjudgments in the time slots occupied by classical signals. Conversely, for quantum signals, the presence of high-pulse classical signals introduces additional noise superimposed on the quantum signals, subsequently impacting the overall performance of QKD. Therefore, we undertake a separate analysis of the noise associated with classical communication and the excess noise in quantum key distribution.

### 1. Noise analysis in classical communication

In our analysis, we denote  $N_0$  as the shot noise, while the coherent-state modulation variance for GMCS modulation is denoted as  $V_A$ , with all subsequent noise variances expressed in shot noise unit (SNU). At the receiver, our protocol is vulnerable to a series of noise sources, including detector noise, relative intensity noise originating from the laser source, phase noise. Consequently, the total noise at the receiver can be formally characterized as [27]

$$N_{\text{tot}} = T\eta[V_A + N_{\text{RIN,sig}} + N_{\text{RIN,LO}}] + 2(1 + V_{\text{el}}), \quad (2)$$

where  $2(1 + V_{\text{el}})$  represents the noise generated by the two detectors in heterodyne detection,  $T$  represents the channel transmittance,  $\eta$  represents the quantum efficiency.

Due to laser spontaneous emission causing fluctuations in photon counting, this variability is considered noise in terms of the laser's amplitude, which we can characterize as relative intensity noise. relative intensity noise can be categorized into the relative noise of the signal and the relative noise of the LO. In Eq. (2),  $N_{\text{RIN,sig}}$  is relative intensity noise of signal, it can be expressed as [3]

$$N_{\text{RIN,sig}} = V_A \sqrt{\text{RIN}_{\text{sig}} \Delta v_A}. \quad (3)$$

At the same time,  $N_{\text{RIN,LO}}$  represents the noise contributed by the relative intensity noise of LO in Eq. (2), it can be expressed as [3]

$$N_{\text{RIN,LO}} = \frac{1}{4} \text{RIN}_{\text{LO}} \Delta v_A V_A. \quad (4)$$

In Eqs. (3) and (4),  $V_A$  represents the modulation variance,  $\text{RIN}_{\text{sig}}$  represents laser relative noise,  $\text{RIN}_{\text{LO}}$  is the relative intensity noise of the local oscillator light, and  $\Delta v_A$  represents the bandwidth of the detector. Here, since  $V_A = 5$  SNUs,  $\text{RIN}_{\text{sig}} = \text{RIN}_{\text{LO}} = 10^{-10} \text{ Hz}^{-1}$ ,  $\Delta v_A = 10 \text{ kHz}$ ,  $N_{\text{RIN,sig}} = 5 \times 10^{-3}$  SNUs,  $N_{\text{RIN,LO}} = 1.25 \times 10^{-6}$  SNUs.

In the preceding theoretical calculation, we derived the noise associated with classical communication using standard parameters. Table I presents the theoretically calculated noise of the classical communication.

### 2. Excess noise in CV-QKD

At the Alice, our protocol is vulnerable to an array of noise sources, including detector noise, the relative noise of

TABLE I. Noise in classical communication.

Noise	Value (in SNUs)
$N_{\text{RIN,sig}}$	$5 \times 10^{-3}$
$N_{\text{RIN,LO}}$	$1.25 \times 10^{-6}$
$V_{\text{el}}$	0.1

the laser, the relative noise of the LO, leakage noise, phase noise, the rest of the excess noise, and analog-to-digital converter (ADC) quantization noise. Concerning the noise at the receiver, which includes electronic noise and shot noise, these are noises generated by well-calibrated detectors that are not under the control of Eve. Hence, we consider them trusted noises. On the other hand, other noises generated at the transmitter are more susceptible to Eve's attacks. Therefore, we regard the associated noises as untrusted [27]. We categorize the shot noise and electronic noise as trustworthy noise, while regarding the relative noise of the laser, the relative noise of the LO, leakage noise, phase noise and the rest of the excess noise as untrustworthy noise. Consequently, the total excess noise at Alice can be formally characterized as [3]

$$\varepsilon_{\text{tot}} = \varepsilon_{\text{RIN,sig}} + \varepsilon_{\text{RIN,LO}} + \varepsilon_{\text{LE}} + \varepsilon_{\text{ph}} + \varepsilon_0 + \frac{\varepsilon_{\text{ADC}}}{T\eta}. \quad (5)$$

In Eq. (5),  $\varepsilon_{\text{RIN,sig}}$  represents the relative intensity noise of laser,  $\varepsilon_{\text{RIN,LO}}$  represents the relative intensity noise of LO. Their theoretical calculation formulas align with those of  $N_{\text{RIN,sig}}$  and  $N_{\text{RIN,LO}}$  in classical communication. Consequently,  $\varepsilon_{\text{RIN,sig}} = N_{\text{RIN,sig}} = 5 \times 10^{-3}$  SNUs,  $\varepsilon_{\text{RIN,LO}} = N_{\text{RIN,LO}} = 1.25 \times 10^{-6}$  SNUs.

In Eq. (5),  $\varepsilon_{\text{LE}}$  represents the leakage noise. In Ref. [15], the high-intensity local oscillator light can leak into the quantum optical signal, introducing additional noise. In comparison to the TLO CV-QKD scheme, our proposed protocol involves only one classical light pulse among the four pulses. Therefore, the leakage noise in our protocol can be expressed as [15]

$$\varepsilon_{\text{LE}} = \frac{A^2}{R_e}, \quad (6)$$

where  $A^2$  represents the optical power of classical signals,  $R_e$  is a finite extinction ratio, we estimate  $\varepsilon_{\text{LE}}$  via commonly employed parameters:  $A^2 = 1500$  SNUs,  $R_e = 65$  dB, so  $\varepsilon_{\text{LE}} = 4.7 \times 10^{-4}$  SNUs.

In Eq. (5),  $\varepsilon_{\text{ph}}$  represents the phase noise. To elaborate, it originates from the laser's spontaneous emission, inducing random frequency fluctuations in the laser pulse signal, resulting in phase drift and subsequently giving rise to phase noise.  $\varepsilon_{\text{ph}}$  can be expressed as [20]

$$\varepsilon_{\text{ph}} = V_A \sigma_{\text{ph}}. \quad (7)$$

In Eq. (7),  $\sigma_{\text{ph}}$  represents the phase drift; it can be expressed as [30]

$$\sigma_{\text{ph}} = 2\pi(\Delta v_S + \Delta v_L)\tau, \quad (8)$$

where  $\Delta v_S$  and  $\Delta v_L$  respectively represent the linewidth of the signal laser and the LO laser, while  $\tau$  denotes the

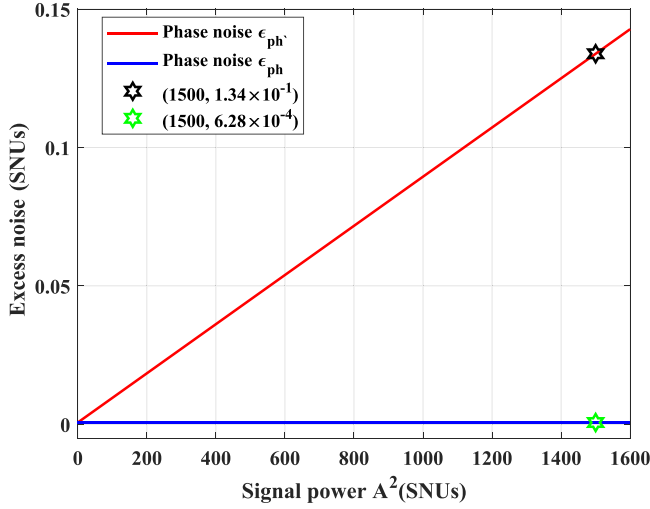


FIG. 3. The phase noise in the GMCS-PPM-SQCC and traditional SQCC protocol. The blue line is the phase noise  $\epsilon_{\text{ph}} = 6.28 \times 10^{-4}$  SNU, the red line represents the relationship between the phase noise of the traditional SQCC protocol and  $A^2$ . The black hexagram represents the coordinate point  $(1500, 1.34 \times 10^{-1})$ , the green hexagram represents the coordinate point  $(1500, 6.28 \times 10^{-4})$ .

time interval between the two pulses. We estimate  $\epsilon_{\text{ph}}$  via commonly employed parameters:  $\tau = 1$  ns,  $\Delta v_S = \Delta v_L = 10$  kHz, so  $\epsilon_{\text{ph}} = 6.28 \times 10^{-4}$  in SNU.

However, in the traditional SQCC protocol, since the quantum signal is superimposed on the classical signal, as the quantum signal is overlaid upon the classical signal, greater amplitudes lead to increased excess noise induced by phase variations. This relationship is expressed as follows [31]:

$$\epsilon_{\text{ph}'} = \left( \frac{A^2}{\sqrt{2}} + V_A \right) \sigma_{\text{ph}'}, \quad (9)$$

where  $\epsilon_{\text{ph}'}$  represents the phase noise of the traditional SQCC protocol,  $A^2$  represents the signal power,  $\sigma_{\text{ph}'}$  represents the phase drift. In the Fig. 3, we present the phase noise for both the conventional SQCC protocol and the GMCS-PPM-SQCC protocol. Specifically, when  $A^2$  is set at 1500 SNU, and when  $\sigma_{\text{ph}'}$  and  $\sigma_{\text{ph}}$  are equal, the phase noise  $\epsilon_{\text{ph}'}$  for the traditional SQCC protocol equals  $1.34 \times 10^{-1}$  SNU.

The last term in Eq. (5), the noise generated by the  $\epsilon_{\text{ADC}}$  can be summarized into two parts, one is the noise generated by the ADC quantization noise  $\epsilon_{\text{ADC}}$  itself, and the other is the noise generated by the  $\epsilon_{\text{ADC}}$  quantization; it can be represented as [20]

$$\epsilon_{\text{ADC}} = \frac{2\tau}{hf(g\rho)^2 P_{\text{LO}}} \left/ \left( \frac{1}{12} \frac{R_U^2 A^2}{2^{2n} V_A} + V_{(\text{ADC}, \text{intr})} \right) \right. \quad (10)$$

Among it,  $n$  is the quantization precision,  $A^2/V_A$  denotes the amplitude ratio between classical signals and quantum signals. In this protocol, increasing the power of classical optical pulses enhances the transmission performance of classical signals. However, the increase in power also results in an elevation of  $\epsilon_{\text{ADC}}$ , necessitating the use of ADC converters that meet the required  $n$  to reduce  $\epsilon_{\text{ADC}}$ . To illustrate the relation-

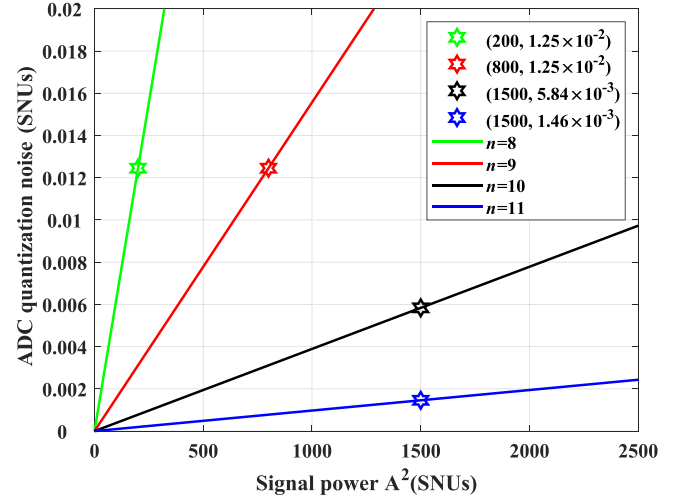


FIG. 4. The relationship between  $\epsilon_{\text{ADC}}$  and  $A^2$ . The parameters involved are  $\tau = 1$  ns,  $f = 193.4$  THz,  $g = 10$  k $\Omega$ ,  $\rho = 0.8$  A/W,  $P_{\text{LO}} = 10$  mW,  $R_U = 0.1$  V,  $V_{(\text{ADC}, \text{intr})} = 10^{-8}$  V $^2$ ,  $A^2 = 1500$  SNU, and  $V_A = 5$  SNU. The green line illustrates the relationship between  $A^2$  and  $\epsilon_{\text{ADC}}$  when the  $n$  is set at eight, the red line illustrates the relationship between  $A^2$  and  $\epsilon_{\text{ADC}}$  when the  $n$  is set at nine, the black line illustrates the relationship between  $A^2$  and  $\epsilon_{\text{ADC}}$  when the  $n$  is set at ten, the blue line illustrates the relationship between  $A^2$  and  $\epsilon_{\text{ADC}}$  when the  $n$  is set at eleven. The green hexagram represents the coordinate point  $(200, 1.25 \times 10^{-2})$ , the red hexagram represents the coordinate point  $(800, 1.25 \times 10^{-2})$ , the black hexagram represents the coordinate point  $(1500, 5.84 \times 10^{-3})$ , the blue hexagram represents the coordinate point  $(1500, 1.46 \times 10^{-3})$ .

ship between  $\epsilon_{\text{ADC}}$  and  $A^2$  under various  $n$ , we can calculate  $\epsilon_{\text{ADC}}$  using standard parameters, where  $\tau = 4$  ns,  $f = 193.4$  THz,  $g = 10$  k $\Omega$ ,  $\rho = 0.8$  A/W,  $P_{\text{LO}} = 8$  mW,  $R_U = 0.1$  V,  $V_{(\text{ADC}, \text{intr})} = 10^{-8}$  V $^2$ ,  $V_A = 5$  SNU. As shown in Fig. 4, when the  $n$  is set at eight and nine,  $\epsilon_{\text{ADC}}$  dramatically increases with rising  $A^2$ . For instance, when  $n$  is set to eight, at  $A^2$  equals 200 SNU, the  $\epsilon_{\text{ADC}}$  has already reached  $1.25 \times 10^{-2}$  SNU. When  $n$  is set to nine, at  $A^2$  equals 800 SNU, the  $\epsilon_{\text{ADC}}$  has also reached  $1.25 \times 10^{-2}$  SNU. However, when the  $n$  exceeds nine, within a certain range, the impact of  $A^2$  on  $\epsilon_{\text{ADC}}$  becomes tolerable. For example, with a  $n$  of ten, at the  $A^2$  of 1500 SNU, the  $\epsilon_{\text{ADC}}$  is  $5.84 \times 10^{-3}$  SNU. Similarly, with a  $n$  of eleven, at the  $A^2$  of 1500 SNU, the  $\epsilon_{\text{ADC}}$  is  $1.46 \times 10^{-3}$  SNU.

In the preceding theoretical calculation, we derived the excess noise in QKD using standard parameters. Table II presents the theoretically calculated excess noise in QKD.

TABLE II. Excess noise in QKD.

Excess noise	Power value (in SNU)
$\epsilon_{\text{RIN}, \text{sig}}$ (untrusted)	$5 \times 10^{-3}$
$\epsilon_{\text{RIN}, \text{LO}}$ (untrusted)	$1.25 \times 10^{-6}$
$\epsilon_{\text{LE}}$ (untrusted)	$4.7 \times 10^{-4}$
$\epsilon_{\text{ph}}$ (untrusted)	$6.28 \times 10^{-4}$
$\epsilon_{\text{ph}'}$ (untrusted)	$1.34 \times 10^{-1}$
$\epsilon_0$ (untrusted)	0.01
$\epsilon_{\text{ADC}}$ (untrusted)	$5.84 \times 10^{-3}$

### B. Performance analysis of classical communication

In GMCS-PPM-SQCC protocol, the BER formula for PPM can be expressed as [32,33]:

$$C_{\text{BER}} = \frac{1}{2} \operatorname{erfc} \left( \frac{1}{2\sqrt{2}} \sqrt{\text{SNR} \times \frac{L}{2} \log_2 L} \right), \quad (11)$$

where  $\operatorname{erfc}(\cdot)$  denotes the complementary error function, defined as  $\operatorname{erfc}(x) = \frac{2}{\sqrt{\pi}} \int_x^\infty e^{-t^2} dt$ , and SNR stands for the signal-to-noise ratio. Here,  $L$  represents the number of time slots in a frame for PPM. The SNR formula can be expressed as [31]

$$\text{SNR} = P/N = T\eta \frac{A^2}{N_{\text{tot}}}. \quad (12)$$

Obviously, with an increase in SNR, the performance of classical communication becomes better. In the classical communication of PPM, the BER will decrease with the increase of the order. We assume that  $L = 4$ , then Eqs. (11) and (12) can be expressed as

$$C_{\text{BER}} = \frac{1}{2} \operatorname{erfc} \left( \sqrt{\frac{T\eta \frac{A^2}{N_{\text{tot}}}}{2}} \right). \quad (13)$$

By Eqs. (12) and (13), we can express the required  $A^2$  as

$$A^2 = \frac{2N_{\text{tot}}[\operatorname{erfc}^{-1}(2C_{\text{BER}})]^2}{T\eta}, \quad (14)$$

where  $T$  can be expressed as the transmittance,  $\eta$  can be expressed as the signal transmission efficiency, where  $T$  can be expressed as

$$T = 10^{(-rl/10)}. \quad (15)$$

As shown in Eq. (15),  $T$  is related to the length of optical fiber  $l$ . According to Eqs. (2), (14), and (15) and Table I, we can establish the correlation between  $l$  and  $A$  as well as the relationship between  $l$  and the BER. As shown in Fig. 5, it can be seen that, when the constrained BER is  $1 \times 10^{-9}$ , a larger value of  $A^2$  corresponds to an extended system transmission distance. Simultaneously, for transmitting the same distance, a higher  $V_A$  requires a greater signal power. Within GMCS-PPM-SQCC protocol, when the  $A^2$  is set at 1500 SNUs, the classical information transmission distance can reach 50 km, maintaining a BER below  $1 \times 10^{-9}$ . It is noteworthy that, in the traditional SQCC protocol [27], the classical information transmission distance also reaches 50 km with BER not exceeding  $1 \times 10^{-9}$  when the  $A^2$  is set at 1500 SNUs.

### C. Performance analysis of CV-QKD

In CV-QKD, the assessment of its performance hinges on the SKR, as computed in the accompanying Appendix. Under this noise model, detector noise  $V_{\text{el}}$ , shot noise and ADC quantization noise  $\varepsilon_{\text{ADC}}$  originate from the system itself and can be regarded as credible noise. In addition, noise contributed by the relative intensity noise of the signal  $\varepsilon_{\text{RIN, sig}}$ , the noise contributed by the relative strength of the local oscillator  $\varepsilon_{\text{RIN, LO}}$ , the phase noise  $\varepsilon_{\text{ph}}$ , and the noise in the channel  $\varepsilon_0$  that is not protected or defined are not credible.

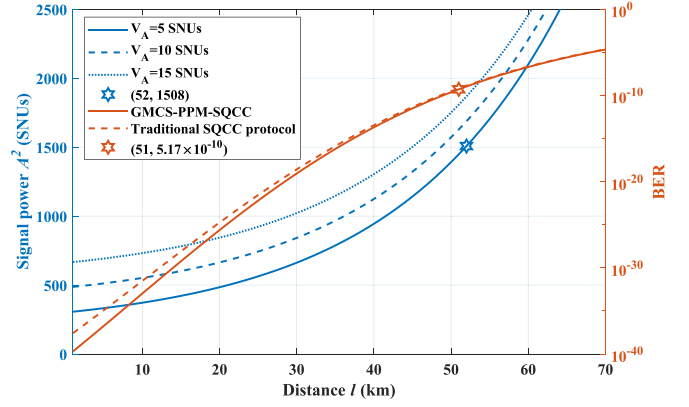


FIG. 5. The relationship of  $A^2$  and  $l$ , as well as the relationship between BER and  $l$ . Attenuation coefficient  $r = 0.2$  dB/km, quantum efficiency  $\eta = 0.6$ . The blue solid and dashed lines depict the relationship between  $A^2$  and  $l$  for different values of  $V_A$  set at 5, 10, and 15 SNUs. The red solid line illustrates the relationship between the BER and the parameter  $l$  in the traditional SQCC protocol, with  $A^2$  set to 1500 SNUs and  $V_A$  set to 5 SNUs. The red dashed line illustrates the relationship between the BER and the parameter  $l$  in the GMCS-PPM-SQCC protocol, with  $A^2$  set to 1500 SNUs and  $V_A$  set to 5 SNUs. The blue hexagram represents the coordinate point (52, 1508), the red hexagram represents the coordinate point (51,  $5.17 \times 10^{-10}$ ).

To elucidate this further, in accordance with Sec. III A, a comparative analysis of the theoretical excess noise between the traditional SQCC protocol and the GMCS-PPM-SQCC protocol is conducted. As illustrated in Fig. 6, The traditional SQCC protocol exhibits higher excess noise compared with the GMCS-PPM-SQCC protocol at a signal power level of 1500 SNUs. To facilitate a more comprehensive performance comparison between the traditional SQCC protocol and the GMCS-PPM-SQCC protocol, we further conduct an analysis of the SKR. The detected noise in the input of Bob's

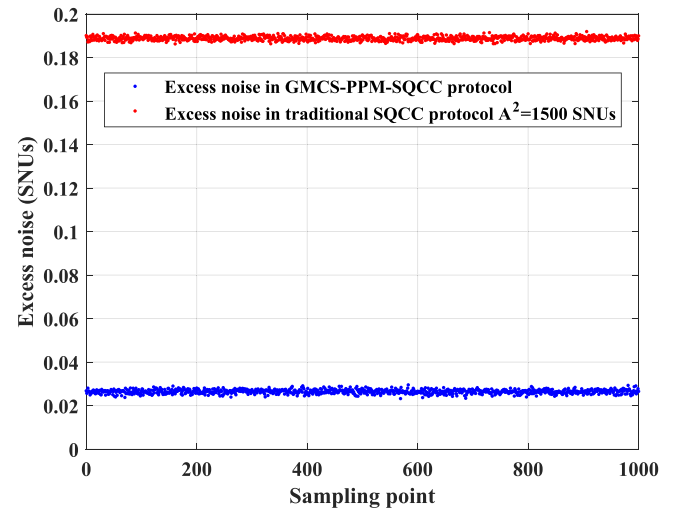


FIG. 6. The excess noise of traditional SQCC protocol and GMCS-PPM-SQCC protocol. The blue dot represents the excess noise of the GMCS-PPM-SQCC protocol. The red dot represents the excess noise of the traditional SQCC protocol.

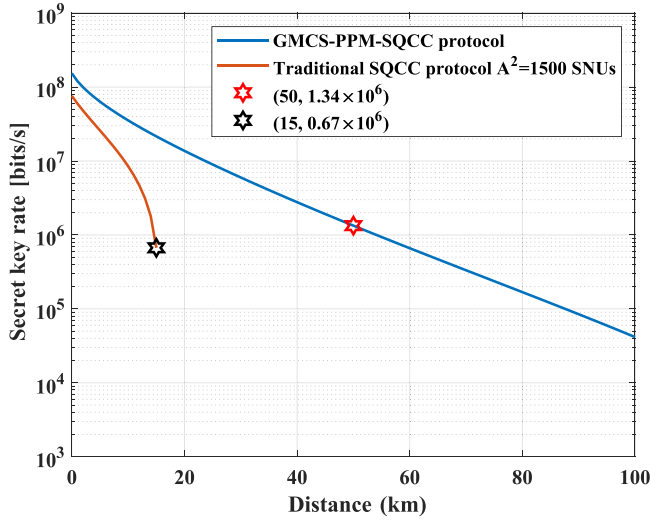


FIG. 7. The SKR at different distances based on GMCS-PPM-SQCC protocol and the traditional SQCC protocol. The blue line represents the relationship between SKR and distance in the GMCS-PPM-SQCC protocol, the red line represents the relationship between SKR and distance in the traditional SQCC protocol. The red hexagram represents the coordinate point  $(50, 1.34 \times 10^6)$ , the black hexagram represents the coordinate point  $(15, 0.67 \times 10^6)$ .

heterodyne detection process can be expressed as

$$\chi_{\text{het}} = [1 + (1 - \eta) + 2V_{\text{el}} + \varepsilon_{\text{ADC}}]/\eta. \quad (16)$$

In a channel, the untrusted noise model can be represented as

$$\chi_{\text{line}} = 1/T - 1 + \varepsilon_0 + \varepsilon_{\text{RIN,sig}} + \varepsilon_{\text{RIN,LO}} + \varepsilon_{\text{ph}}, \quad (17)$$

and the total noise of the channel input can be expressed as

$$\chi_{\text{tot}} = \chi_{\text{line}} + \frac{\chi_{\text{het}}}{T}. \quad (18)$$

Based on the preceding analysis, we can compute the SKR achievable by the CV-QKD system employing the PPM-GMCS-SQCC protocol. In our calculations, we consider specific parameters, such as the repetition rate  $f_s = 250$  MHz,  $A^2 = 1500$  SNU,  $V_A = 5$  SNU, reconciliation efficiency  $\beta = 90\%$ , attenuation coefficient  $R = 0.2$  dB/km, and quantum efficiency  $\eta = 0.6$ .

In Fig. 7, we compare the SKR of the GMCS-PPM-SQCC protocol with that of the traditional SQCC protocol, as computed in the accompanying Appendix. At a distance of 50 km, the SKR of GMCS-PPM-SQCC protocol reaches 1.34 Mbps. In comparison, the SKR of the traditional SQCC protocol only achieves 0.67 Mbps at a distance of 15 km.

#### IV. DISCUSSION

This paper introduces an SQCC protocol named GMCS-PPM-SQCC protocol, which integrates PPM for classical communication and GMCS for CV-QKD. In this protocol, classical information is conveyed within specific time slots of a frame using classical light pulses, while the remaining slots are allocated for quantum information transmission. This segregation ensures that the transmission of classical signals has no adverse impact on the performance of quantum signals. By establishing a comprehensive noise model, we conduct a

performance analysis comparing the traditional SQCC protocol with the GMCS-PPM-SQCC protocol.

Simulation results reveal that when the  $A^2$  is set at 1500 SNU and the  $V_A$  is 5 SNU, classical signals in the GMCS-PPM-SQCC protocol can be transmitted over a 50 km distance with a BER below  $1 \times 10^{-9}$ . Concurrently, the theoretical SKR for the GMCS-PPM-SQCC protocol reaches 1.61 Mbps at 50 km, whereas the SKR of the traditional SQCC protocol only achieves 0.67 Mbps at a distance of 15 km. It is evident that the performance of the traditional SQCC protocol is inferior to GMCS-PPM-SQCC. This difference arises because, in the traditional SQCC protocol, classical and quantum signals are simultaneously encoded on quadrature components. Moreover, as the power of classical signals increases, so does the phase noise. In contrast, in the GMCS-PPM-SQCC protocol, classical and quantum signals are temporally separated within a frame, preventing classical signals from interfering with the phase of quantum signals. In contrast, the GMCS-PPM-SQCC protocol places classical and quantum signals in different time slots, preventing classical signals from interfering with the phase noise of quantum signals. The advantages of the GMCS-PPM-SQCC protocol not only simplify system complexity and enhance key transmission rates but also fortify the stability of simultaneous quantum and classical communication.

In the analysis of ADC quantization noise and leakage noise in Sec. III A 2 of the paper, we conducted simulations using commercially available analog-to-digital converters with appropriate quantization precision and optical devices with common extinction ratios. To effectively suppress excess noise and ensure the SKR, it is necessary to carefully choose the classical signal power for classical signal transmission. However, this entails sacrificing a portion of the classical signal transmission performance. Certainly, in scenarios without considerations for actual experimental costs, opting for high-precision analog-to-digital converters and optical devices with high extinction ratios to suppress excess noise does not necessarily lead to an enhancement in quantum communication performance while compromising classical communication. Instead, it is possible to simultaneously reduce excess noise and opt for higher classical signal power, enabling both modes of communication to achieve superior performance.

The initial concept behind our proposed protocol is to encode information by utilizing various parameters of the coherent state. One can consider implementing this protocol by combining the polarization state with quadrature components. In the simultaneous quantum and classical communication, a polarization-based approach involving the combination of polarization states and quadrature components can be considered. Specifically, classical information is transmitted through the polarization direction of coherent states modulated with a Gaussian distribution. When the polarization direction is set to horizontal (H), the classical information is encoded as “1”; when the polarization direction is vertical (V), the classical information is encoded as “0.” At the receiver, the polarization direction is employed to discern classical information, while the quadrature component is utilized for key extraction.

However, challenges arise when quantum signals reach the receiver, as they are exceedingly weak, making it difficult



to accurately determine the polarization direction. Simultaneously, variations in polarization introduce errors in the classical signal, and correcting these errors becomes challenging due to the low SNR of quantum signal.

We can also consider implementing this protocol through separate modes of a two-mode state. Specifically, in a two-mode state, where one mode is utilized for classical communication, while another mode is dedicated to quantum communication, and signal transmission is facilitated through multimode optical fibers. Entanglement correlations within this setup may play a role in noise reduction.

## V. CONCLUSION

GMCS-PPM-SQCC is an attractive protocol. It supports classical communication and CV-QKD can be transmitted in the same communication infrastructure, which can greatly reduce the transmission cost of CV-QKD and promote the wide application of quantum key distribution. In PPM, the main difference from classical modulation lies in the fact that in addition to the light pulses, which represent classical information, the remaining time slots carry quantum key information.

Moreover, classical communication typically necessitates higher optical power, while quantum communication demands the lowest possible transmit power for security assurance. Therefore, schemes based on pulse position modulation can be particularly advantageous in scenarios with stringent power constraints, ultimately extending the lifespan of the power source. Additionally, because classical signals and quantum signals are in different time slots, the transmission of classical information has little impact on the transmission performance of quantum information, making it well-suited for quantum communication applications.

Although this scheme incurs some bandwidth loss, it offers several advantages compared with the traditional SQCC protocol. During transmission, the average optical power is lower, and the power of classical signals does not induce additional phase drift. Consequently, there is no need for supplementary postprocessing for phase recovery. Its security has been verified, and it offers an improved cost-efficiency ratio, making it better suited for signal encapsulation in quantum network applications.

## ACKNOWLEDGMENTS

This work is supported by the National key research and development program (Grant No. 2016YFA0302600), National Natural Science Foundation of China (Grants No.

62101320, No. 61671287, and No. 61971276), Shanghai Municipal Science and Technology Major Project (Grant No. 2019SHZDZX01), and the Key R&D Program of Guangdong province (Grant No. 2020B030304002).

## APPENDIX: CALCULATION OF SECRET KEY RATE

Here we derive the formula for the SKR. First, the mutual information shared between Alice and Bob denoted  $I_{AB}^{\text{het}}$ , and the maximum information available to Eve regarding Bob's key, represented as  $\chi_{BE}^{\text{het}}$ , can be expressed as follows due to the use of heterodyne detection in this paper. Under asymptotic conditions, the reverse reconciliation relationship of SKR can be expressed as [34]

$$R = \beta I_{AB}^{\text{het}} - \chi_{BE}^{\text{het}}, \quad (\text{A1})$$

where  $\beta$  represents reverse negotiation efficiency,  $\beta \in (0, 1)$ ,  $I_{AB}^{\text{het}}$  and  $\chi_{BE}^{\text{het}}$  can be identified as

$$I_{AB}^{\text{het}} = 2 \frac{1}{2} \log_2 \frac{V + \chi_{\text{tot}}}{1 + \chi_{\text{tot}}},$$

$$\chi_{BE}^{\text{het}} = \sum_{i=1}^2 G\left(\frac{\lambda_i - 1}{2}\right) - \sum_{i=3}^5 G\left(\frac{\lambda_i - 1}{2}\right), \quad (\text{A2})$$

where  $V$  is the vacuum state variance of the bimodal squeezed state,  $V = V_A + 1$ ,  $\chi_{\text{tot}}$  represents the total noise of channel input,  $G(x) = (x + 1) \log_2(x + 1) - x \log_2 x$ ,  $\lambda_i$  is the symplectic eigenvalue derived from the covariance matrix and can be defined as

$$\lambda_{1,2}^2 = \frac{1}{2}(A \pm \sqrt{A^2 - 4B}),$$

$$\lambda_{3,4}^2 = \frac{1}{2}(C \pm \sqrt{C^2 - 4D}),$$

$$\lambda_5 = 1, \quad (\text{A3})$$

where

$$A = V^2(1 - 2T) + 2T + T^2(V + \chi_{\text{line}})^2,$$

$$B = T^2(V \chi_{\text{line}} + 1)^2,$$

$$C = \frac{1}{[T(V + \chi_{\text{tot}})]^2} [A \chi_{\text{het}}^2 + B + 1$$

$$+ 2\chi_{\text{het}}(V\sqrt{B} + T(V + \chi_{\text{line}})) + 2T(V^2 - 1)],$$

$$D = \left(\frac{V + \sqrt{B}\chi_{\text{het}}}{T(V + \chi_{\text{tot}})}\right)^2. \quad (\text{A4})$$

According to the above calculation formula, the SKR is eventually evaluated.

- [1] F. Grosshans and P. Grangier, *Phys. Rev. Lett.* **88**, 057902 (2002).
- [2] F. Grosshans, G. Van Assche, J. Wenger, R. Brouri, N. J. Cerf, and P. Grangier, *Nature (London)* **421**, 238 (2003).
- [3] F. Laudenbach, C. Pacher, C.-H. F. Fung, A. Poppe, M. Peev, B. Schrenk, M. Hentschel, P. Walther, and H. Hübel, *Adv. Quantum Technol.* **1**, 1800011 (2018).

- [4] R. García-Patrón and N. J. Cerf, *Phys. Rev. Lett.* **97**, 190503 (2006).
- [5] M. Navascués, F. Grosshans, and A. Acín, *Phys. Rev. Lett.* **97**, 190502 (2006).
- [6] J. Lodewyck, M. Bloch, R. García-Patrón, S. Fossier, E. Karpov, E. Diamanti, T. Debuisschert, N. J. Cerf, R. Tualle-Brouri, S. W. McLaughlin *et al.*, *Phys. Rev. A* **76**, 042305 (2007).

- [7] S. Pirandola, S. L. Braunstein, and S. Lloyd, *Phys. Rev. Lett.* **101**, 200504 (2008).
- [8] R. Renner and J. I. Cirac, *Phys. Rev. Lett.* **102**, 110504 (2009).
- [9] A. Leverrier, F. Grosshans, and P. Grangier, *Phys. Rev. A* **81**, 062343 (2010).
- [10] F. Furrer, T. Franz, M. Berta, A. Leverrier, V. B. Scholz, M. Tomamichel, and R. F. Werner, *Phys. Rev. Lett.* **109**, 100502 (2012).
- [11] A. Leverrier, R. García-Patrón, R. Renner, and N. J. Cerf, *Phys. Rev. Lett.* **110**, 030502 (2013).
- [12] A. Leverrier, *Phys. Rev. Lett.* **114**, 070501 (2015).
- [13] A. Leverrier, *Phys. Rev. Lett.* **118**, 200501 (2017).
- [14] P. Jouguet, S. Kunz-Jacques, A. Leverrier, P. Grangier, and E. Diamanti, *Nat. Photon.* **7**, 378 (2013).
- [15] D. Huang, P. Huang, D. Lin, and G. Zeng, *Sci. Rep.* **6**, 19201 (2016).
- [16] C. Wang, D. Huang, P. Huang, D. Lin, J. Peng, and G. Zeng, *Sci. Rep.* **5**, 14607 (2015).
- [17] Y. Zhang, Z. Li, Z. Chen, C. Weedbrook, Y. Zhao, X. Wang, Y. Huang, C. Xu, X. Zhang, Z. Wang *et al.*, *Quantum Sci. Technol.* **4**, 035006 (2019).
- [18] M. Ziebell, M. Persechino, N. Harris, C. Galland, D. Marris-Morini, L. Vivien, E. Diamanti, and P. Grangier, in *The European Conference on Lasers and Electro-Optics, Munich, Germany* (Optica Publishing Group, 2015), p. JSV\_4\_2.
- [19] G. Zhang, J. Y. Haw, H. Cai, F. Xu, S. M. Assad, J. F. Fitzsimons, X. Zhou, Y. Zhang, S. Yu, J. Wu *et al.*, *Nat. Photon.* **13**, 839 (2019).
- [20] L. Li, T. Wang, X. Li, P. Huang, Y. Guo, L. Lu, L. Zhou, and G. Zeng, *Photon. Res.* **11**, 504 (2023).
- [21] D. Huang, P. Huang, H. Li, T. Wang, Y. Zhou, and G. Zeng, *Opt. Lett.* **41**, 3511 (2016).
- [22] P. Eraerds, N. Walenta, M. Legré, N. Gisin, and H. Zbinden, *New J. Phys.* **12**, 063027 (2010).
- [23] K. A. Patel, J. F. Dynes, M. Lucamarini, I. Choi, A. W. Sharpe, Z. L. Yuan, R. V. Pentty, and A. J. Shields, *Appl. Phys. Lett.* **104**, 051123 (2014).
- [24] Y. Mao, B.-X. Wang, C. Zhao, G. Wang, R. Wang, H. Wang, F. Zhou, J. Nie, Q. Chen, Y. Zhao *et al.*, *Opt. Express* **26**, 6010 (2018).
- [25] B. Qi, *Phys. Rev. A* **94**, 042340 (2016).
- [26] Y. Gong, R. Kumar, A. Wonfor, R. Pentty, and I. White, in *CLEO: Applications and Technology, San Jose, CA, USA* (Optica Publishing Group, 2018), p. JTh2A.23.
- [27] B. Qi and C. C. W. Lim, *Phys. Rev. Appl.* **9**, 054008 (2018).
- [28] Y. Zhang, Z. Chen, S. Pirandola, X. Wang, C. Zhou, B. Chu, Y. Zhao, B. Xu, S. Yu, and H. Guo, *Phys. Rev. Lett.* **125**, 010502 (2020).
- [29] A. Aguado, V. Lopez, D. Lopez, M. Peev, A. Poppe, A. Pastor, J. Folgueira, and V. Martin, *IEEE Commun. Mag.* **57**, 20 (2019).
- [30] A. Marie and R. Alléaume, *Phys. Rev. A* **95**, 012316 (2017).
- [31] T. Wang, P. Huang, S. Wang, and G. Zeng, *Phys. Rev. A* **99**, 022318 (2019).
- [32] T. Y. Elgarnimi, *Int. J. Comput. Appl.* **79**, 22 (2013).
- [33] S. Trisno, *Design and Analysis of Advanced Free Space Optical Communication Systems* (University of Maryland, College Park, 2006).
- [34] S. Fossier, E. Diamanti, T. Debuisschert, R. Tualle-Brouiri, and P. Grangier, *J. Phys. B: At. Mol. Opt. Phys.* **42**, 114014 (2009).